Geophysical Research Letters

RESEARCH LETTER
10.1029/2022GL102385

**Key Points:**

- Microstructures of deformed talc indicate that talc retains a frictional control on deformation at high pressure and temperature
- Constant indentation hardnesses with respect to strain suggest that strain-induced talc microstructures do not affect material strength
- Nanoporosity generated at high strains could accommodate fluids in fault zones

**Correspondence to:**
C. M. Horn,
cmhorn@wustl.edu

**Citation:**
Horn, C. M., & Skemer, P. (2023). Semi-brittle deformation of talc at the base of the seismogenic zone. *Geophysical Research Letters*, *50*, e2022GL102385. https://doi.org/10.1029/2022GL102385

Received 2 DEC 2022
Accepted 28 MAR 2023

**Author Contributions:**
**Conceptualization:** P. Skemer
**Formal analysis:** C. M. Horn, P. Skemer
**Funding acquisition:** P. Skemer
**Investigation:** C. M. Horn
**Writing – original draft:** C. M. Horn, P. Skemer
**Writing – review & editing:** C. M. Horn, P. Skemer



# Semi-Brittle Deformation of Talc at the Base of the Seismogenic Zone

**C. M. Horn**[1] **and P. Skemer**[1]

[1]Department of Earth & Planetary Sciences, Washington University in St Louis, Saint Louis, MO, USA

**Abstract** Talc is commonly found in the cores of exhumed faults and may be important to the dynamics of slip in active fault zones. To understand the rheology of talc at conditions relevant to subduction zones, we conducted torsional deformation experiments at high pressure (1 GPa) and temperatures (450–500°C). Scanning Transmission Electron Microscope imaging revealed a marked decrease in grain size with increasing strain, in addition to the development of grain kinking and nanoporosity. The similarity of these microstructures to talc deformed in natural faults and low-pressure experiments indicates that the dominant deformation mechanisms of talc are similar across a wide range of depths. We conclude that frictional processes remain an important control on talc rheology even under high normal stresses. However, deformation-induced porosity could enhance the percolation of high-pressure or reactive fluids through talc-rich lithologies.

**Plain Language Summary** Talc, an extremely weak mineral commonly observed in natural faults, likely plays an important role in controlling how earthquake-generating faults slip. We performed high pressure deformation experiments on a natural talc sample to help understand the role of talc at depth in large faults. Many minerals will undergo a change in deformation style as pressure and temperature increase, from a mechanism controlled by friction to a mechanism controlled by defects within the crystal lattice. Conversely, our findings indicate that talc does not experience a change in deformation mechanism at high pressure and temperature, with friction remaining an important control on talc deformation across all our experiments. This suggests that talc remains brittle throughout the seismogenic zone, including the region of tremor and slow slip. However, we also observed that as strain in the talc increased so did the generation of pore space in the samples. This could increase permeability, allowing fluids to migrate more readily through deformed talc.

## 1. Introduction

Talc, a hydrous magnesium silicate, may hold the key to understanding why some faults continue to accommodate strain even when subjected to low resolved shear stresses (Byerlee, 1978; Collettini et al., 2009; Escartín et al., 2003; Moore & Rymer, 2007; Viti & Collettini, 2009; Wibberley, 2007). Talc is extremely weak, with both internal and sliding frictional coefficients in the range $0.08 \leq \mu \leq 0.36$ (Escartín et al., 2008; Hirauchi, 2013; Misra et al., 2014; Moore & Lockner, 2008, 2011; Morrow et al., 2000). Talc has been documented in many fault zone environments (Bonatti et al., 1971; Boschi et al., 2006; Moore & Rymer, 2007) and is known to form in subduction zones through the hydration and/or silica metasomatism of mafic rocks (Kim et al., 2013; King et al., 2003; Spandler et al., 2008). Its wide stability field (Pawley & Wood, 1995) overlaps important seismically active regions of a subduction zone, including the seismogenic zone, the inferred source region for tremor and slow slip events (SSEs), and intermediate-depth earthquakes (Figure 1). In this study, we investigate the response of polycrystalline talc to high-strain deformation under pressure, temperature, and strain-rate conditions that are nearly identical to the conditions at the subduction zone interface where slow slip occurs (Rowe et al., 2011; Syracuse et al., 2010). Even at these high pressure and temperature conditions, deformed specimens reveal microstructures indicative of semi-brittle deformation processes and a frictional control on talc rheology. Notably, we observe the formation of delaminations and ripplocations, features that introduce porosity. The porosity generated during semi-brittle deformation could enable the circulation of high-pressure fluids.

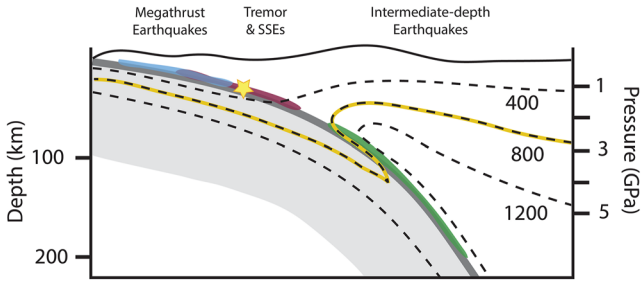


**Figure 1.** Schematic of a hot subduction zone. Temperature contours are from Currie et al. (2004). The pale gray region represents the downgoing slab, with depths dominated by different seismic regimes highlighted atop the slab. The yellow star indicates the pressure at which our experiments were conducted. The maximum depth of talc is assumed to follow the 800°C isotherm (highlighted in yellow), since in a hot subduction environment talc stability will be exceeded before it reaches its maximum pressure limit (Pawley & Wood, 1995). Earthquake depths are from Schwartz and Rokosky (2007) and Hyndman et al. (1997).

## 2. Methods

### 2.1. Torsion Experiments

High strain torsional deformation experiments on talc were conducted using the solid medium Large Volume Torsion (LVT) apparatus at Washington University in St Louis (see Cross and Skemer (2017) for more details on the experimental apparatus and procedure). The starting material for these experiments was natural polycrystalline talc specimens from Van Horn, Texas, which were purchased from Ward's Natural Science. X-Ray Diffraction analysis showed the specimens to be approximately 90% talc with 10% dolomite and <1% quartz. The specimens are also weakly foliated. Since the specimens were fragile, half cylinders of radius 2.1 mm were milled from the starting material using a Roland Modela MDX-40A milling machine using carbide end mills. These half cylinders were then sliced perpendicular to the long axis into semi-circular disc-shaped samples of height 1.5–2.1 mm. A layer of gold was sputtered onto the adjoining faces of the half discs to serve as a passive strain marker. Two half disc samples were placed between two hard fired pyrophyllite pistons and loaded into a furnace and gasket assembly

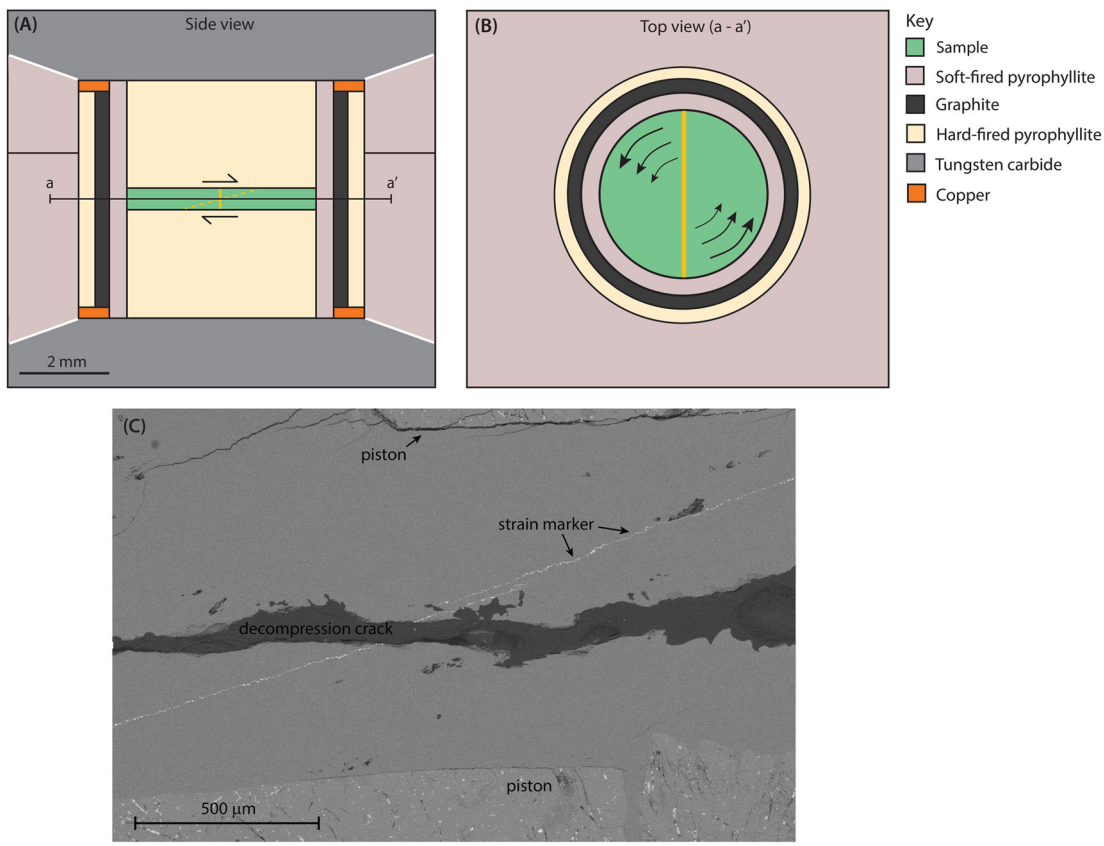


**Figure 2.** (a) Schematic cartoon of the deformation cell. Side view of the cell sandwiched between the tungsten carbide forcing anvils. Arrows indicate the direction of shear that is imposed on the sample. The strain marker starts in a vertical orientation (solid yellow line) and evolves to an inclined angle (dashed yellow line) as deformation progresses. The profile a-a′ is shown in a top-down orientation in (b). (b) Top-down view of the deformation cell. The arrows illustrate how the strain gradient changes from the outer edges of the sample (maximum strain) to the center (minimum strain). (c) Backscattered electron image of the $\gamma = 5.7$ experiment (Large Volume Torsion 357). The gold strain marker can be seen in white at an angle of 10° to the horizontal. A lack of sudden changes in gradient indicates that there has been no strain localisation or macroscopic faulting in the sample. Decompression cracks form during unloading of the experiment and are subsequently filled with epoxy (dark gray).

(Figures 2a and 2b). Experimental assemblies were stored in a vacuum oven at 110°C for 2–12 hr to eliminate any adsorbed water before they were loaded into the LVT apparatus for deformation.

Experiments were conducted at a constant axial load equivalent to 1 GPa and heated to a temperature of 450–500°C. Specimens were not encapsulated and experiments were conducted under fluid-free conditions. Due to the torsional geometry no thermocouple was used during the experiment and temperature was controlled by setting and maintaining constant power to the graphite furnace. Pressure in the center of the sample (upper limit) was estimated from the Bismuth I-II phase transition and found to be 2.45 GPa, with pressure around the edge of the sample (lower limit) calculated by conservatively considering the load to be evenly distributed across the whole gasket (40 mm diameter) and found to be 0.4 GPa. Assuming that there is a linear pressure increase from the inner diameter of the gasket to the center, the pressure at the point where samples were prepared for microstructural analysis is ~1 GPa. These conditions were selected to be complementary to lower pressure experiments at similar temperatures (Escartín et al., 2008; Misra et al., 2014) in order to simulate the response of talc to deformation at greater depths within the earth. Deformation was imposed by twisting at a constant rate of $1.3 \times 10^{-5}$–$1.3 \times 10^{-4}$ rad $s^{-1}$, resulting in an estimated maximum shear strain rate of $1 \times 10^{-5}$–$1 \times 10^{-14}$ $s^{-1}$ at the outer radius of the specimen. As some sliding occurs between the sample, the pistons, and the forcing anvils, the angle of rotation of the gold strain markers is used to confirm the total strain experienced by each experimental sample. As the LVT is optimized for high temperature, high pressure, high strain experiments on relatively large samples, we are unable to collect precise stress and strain data in situ.

### 2.2. Scanning Transmission Electron Microscopy

After each experiment talc specimens were first impregnated with epoxy before being cut into tangential and axial sections. These sections were remounted into 1" rounds before being ground flat and parallel on both sides using 240 grit SiC sandpaper. The side of interest was subsequently polished using a 1 μm diamond impregnated polishing film. The large jump in grit size helped to ensure the sample remained flat, as the difference in hardness between the pyrophyllite pistons and the talc sample often lead to the talc being preferentially removed. Following the 1 μm step, any large scratches remaining were removed by 6+ hours of polishing with colloidal silica using a Buehler MiniMet automatic polishing machine. These samples were then carbon coated, before fabricating several thin foils (~10 μm × 20 μm × 300 nm) using a Thermofisher Scios 2 Focused Ion Beam in the Institute of Materials Science and Engineering at Washington University in St Louis. The surface of the sample was protected by a 1 μm thick rectangle of amorphous platinum. Initial cutting was performed using the ion beam at 30 kV and 5 nA, followed by a series of polishing steps at decreasing voltage to remove any amorphous material formed at high voltage. The resulting lamellae were mounted on Cu half-grids for analysis using Scanning Transmission Electron Microscopy (STEM).

STEM imaging was carried out using a JEOL 2100F Transmission Electron Microscope (TEM), also in the Institute of Materials Science and Engineering. Samples are extremely beam sensitive and rapidly degraded under normal TEM imaging conditions, so STEM images were collected with a camera length of 20 cm at beam conditions of 200 kV and a current of 163 μA, corresponding to a spot size of 0.2 nm.

### 2.3. Nanoindentation

Deformation experiments were further analyzed using nanoindentation to investigate how strain-induced microstructures affected the mechanical properties of the material. Nanoindentation was employed because conventional diffraction-based methods proved unsuccessful at analyzing the development of microstructure, including crystallographic alignment with increasing strain, due to the small grain-size and high degree of crystal distortion introduced during deformation. Experiment halves that were not used for TEM analysis were polished to the same specifications for use in nanoindentation experiments. Flat, polished samples were attached to polished steel discs using strips of tape over the corners of the samples. Load-controlled nanoindentation testing was conducted at room temperature in a Hysitron TI 950 TriboIndenter equipped with a diamond-tipped Berkovich probe and magnetic stage in the McKelvey School of Engineering at Washington University in St Louis. Humidity was kept constant at 49% relative humidity. Individual indentation experiments consisted of a 2s loading phase to a maximum load of 2 mN, a 2s hold period and a 2s unloading phase. This loading pattern was selected to generate indents that are sufficiently deep to ensure that misshapen or

**Table 1**
*Experimental Data*

Summary of Experimental Data

| Sample | IGSN | Strain rate ($s^{-1}$) | Total Strain ($\gamma$) | Number of Successful Indents | | Mean Hardness (GPa) | | Mean Reduced Modulus (Gpa) | |
|---|---|---|---|---|---|---|---|---|---|
| | | | | Parallel to shear plane normal | Perpendicular to shear plane normal | Parallel to shear plane normal | Perpendicular to shear plane normal | Parallel to shear plane normal | Perpendicular to shear plane normal |
| LVT 325 | IESPM0069 | $1.7 \times 10^{-5}$ | $8.1^{+1.4}_{-1.0}$ | 195 | 191 | 0.35 ± 0.18 | 0.78 ± 0.29 | 7.5 ± 2.4 | 14.6 ± 3.4 |
| LVT 329 | IESPM006J | $2.1 \times 10^{-6}$ | $1.0^{+0.1}_{-0.1}$ | 196 | 166 | 0.58 ± 0.28 | 0.65 ± 0.24 | 10.2 ± 4.8 | 21.1 ± 5.5 |
| LVT 342 | IESPM006Z | $6.1 \times 10^{-5}$ | $3.5^{+0.2}_{-0.2}$ | 184 | 193 | 0.34 ± 0.12 | 0.59 ± 0.18 | 6.6 ± 1.8 | 16.6 ± 4.2 |
| LVT 349 | IESPM007B | $4.5 \times 10^{-6}$ | $1.4^{+0.1}_{-0.1}$ | 187 | 191 | 0.61 ± 0.22 | 0.76 ± 0.24 | 15.1 ± 3.4 | 18.4 ± 6.0 |
| LVT 357 | IESPM007H | $1.4 \times 10^{-5}$ | $5.7^{+0.6}_{-0.6}$ | 185 | 196 | 0.31 ± 0.08 | 0.92 ± .34 | 4.1 ± 1.5 | 14.7 ± 4.3 |
| LVT 360 | IESPM007L | 0 | 0 | 196 | 189 | 0.45 ± 0.18 | 0.57 ± 0.09 | 10.2 ± 2.7 | 13.4 ± 2.3 |
| Epoxy | n/a | n/a | n/a | 100 | | 0.31 ± 0.01 | | 5.1 ± 0.1 | |

*Note*. IGSN (=International Geo Sample Number) are the reference numbers for the online specimen catalog https://www.geosamples.org/. Errors for the hardnesses and reduced elastic moduli are reported as 1 std. Strain rate is calculated assuming the specimen deformed at a constant rate of slip for the duration of theexperiment.

broken probe tips do not affect the data. Deep indents (maximum depth ~200–700 nm), coupled with the small grain size (between ~3 and 5 μm and <0.1 μm, depending on strain) also ensured that each individual indent sampled many grains, and thus accurately reflected the bulk strength of the material. Indentation testing of the epoxy used to impregnate the samples revealed that it had a mean hardness of 0.31 ± 0.01 GPa and a mean reduced modulus of 5.1 ± 0.1 GPa. As these numbers are either lower than or equal to the lowest talc values, we take the data for talc reported using this method to be a lower limit to the true hardness and reduced modulus of talc. For further information regarding details of the calculation of indentation hardness and reduced elastic modulus, including how the two properties are related to yield stress and Young's modulus, respectively, see Sly et al. (2020).

After polishing, the edges of the 1" rounds were trimmed so that samples measured roughly 5 × 5 mm. When we had finished testing in the tangential orientation (with the axis of indentation parallel to the shear plane), the same samples were re-cut and polished to expose talc material orthogonal to the shear plane so that the axis of indentation became perpendicular to the shear plane (parallel to the shear plane normal). Any flexure that could have been caused by gaps between the sample back and steel disc was eliminated by careful polishing to ensure that both sample and disc were flat and parallel.

## 3. Results

Six successful torsion experiments were selected for analysis, with observed strains from $0 \leq \gamma \leq 8$ (Table 1). Scanning Transmission Electron Microscopy (STEM) imaging reveals a trend of increasing microstructural damage with strain, including grain-size reduction and the kinking and delamination of crystal lattices (Figure 3). Talc in zero strain sample, which was taken up to the relevant pressures and temperatures and held at these conditions for 1 day without deformation prior to quenching and unloading, has relatively large and elongate grains (~3–5 μm in length), with straight margins parallel to the (001) planes (Figure 3a). No porosity was observed in this sample. However, even moderate shear strains ($\gamma = 1$) are sufficient to introduce sinuous grain margins and some incipient grain size reduction (Figure 3b). Further deformation causes grain sizes to decrease to <0.5 μm, with observable kinking in the crystal lattices (defined here as initially undistorted grains folded about a distinct axis in an angular manner). Kinking of the crystal lattices is often associated with the development of porosity in the hinges of these kinks (Figure 3c). By $\gamma = 8$ the sample has developed a strong foliation with the talc (001) planes subparallel to the shear plane (Figure 3e). In addition, we observe (001) delaminations (where the basal planes of talc can be seen to be peeling apart from one another) and the formation of ripplocations ("ripple dislocations," wherein a layered material deforms by elastic flexure of individual layers (Kushima et al., 2015)) (Figures 3g and 3f). We see no offsets in the passive strain marker (Figure 2c) that would indicate strain localisation or brittle macroscopic failure on the scale of our specimens–rather, deformation is distributed

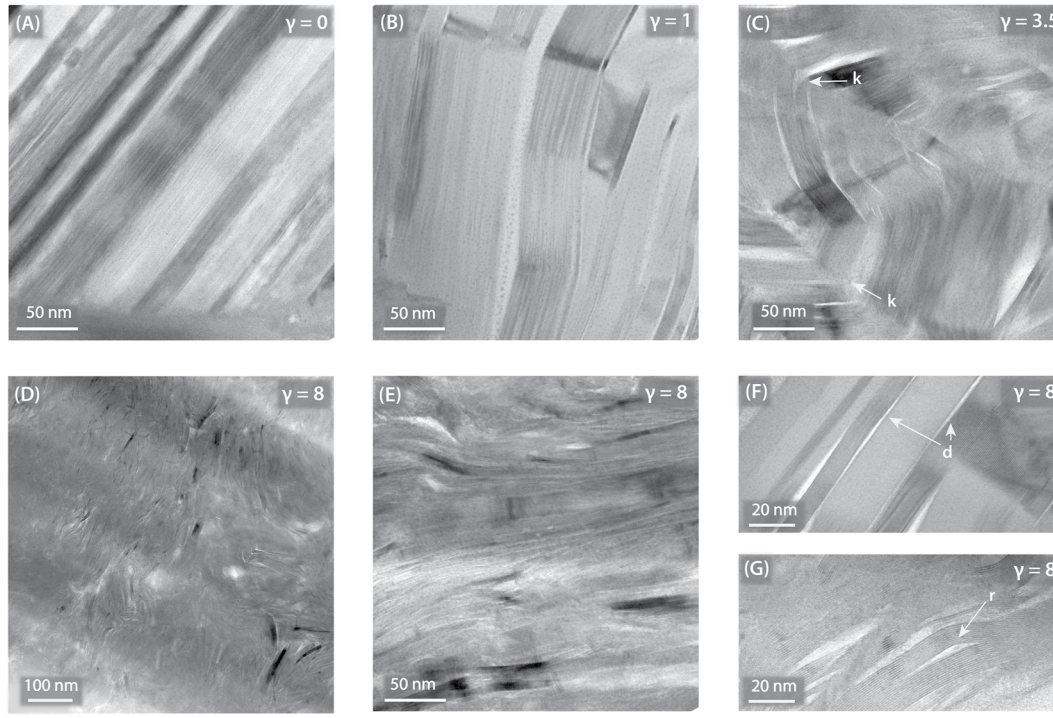


**Figure 3.** Bright field Scanning Transmission Electron Microscopy images of talc deformed from $0 \leq \gamma \leq 8$, showing the evolution of grain size and the development of microporosity with increasing strain. As strain increases, the grain size decreases and there is an increase in grain kinking and delamination. (a–c), (e) are all at the same magnification with the shear plane horizontal. (d and g) are from a Transmission Electron Microscope foil made at a low angle to the shear plane, allowing the foil to intersect with features aligned within the shear plane several times. Grain sizes of <0.1 μm can clearly be seen in (d). The fold axes of kinked grains are indicated by (k) in (c), after the description of kinked grains given by Escartin et al. (2008). (f) Is from a slightly coarser-grained region of the high strain sample, in which delaminations (d) can clearly be seen. A ripplocation (r) is marked in (g).

homogeneously across the entire deformation specimen. In all cases, deformation microstructures are uniform across the TEM sections (10 μm × 20 μm × 300 nm).

To compliment the torsional deformation experiments we also performed a series of room temperature nanoindentation experiments on the deformed talc specimens to assess how increasing shear strain and microstructural damage affects the mechanical strength of talc-bearing rocks (Figure 4). Indents in the strained talc return low hardnesses ($0.3\ \text{GPa} \leq H_{mean} \leq 0.9\ \text{GPa}$) that do not change within error as strain increases. Conversely, the values for the reduced modulus ($4.1 \leq Er_{mean} \leq 21.1\ \text{GPa}$) diverge at higher strains.

## 4. Discussion

Despite its potential importance to fault zone dynamics, little is known about the high-pressure rheology of the mineral talc ($Mg_3Si_4O_{10}(OH)_2$). Previously published experimental work on talc microstructures were conducted at confining pressures that range from 0.1 to 0.3 GPa (Escartín et al., 2008; Misra et al., 2014), corresponding to depths in Earth of up to approximately 10 km. However, natural talc at conditions relevant to SSEs experiences pressures up to ~1.5 GPa (Bürgmann, 2018; Hyndman et al., 1997; Schwartz & Rokosky, 2007) (50 km depth), and the associated normal stresses on shear zones where SSEs occur is assumed to supress cavitation and other brittle/frictional phenomena (Brace et al., 1968; Paterson, 1958). In our experiments, conducted in a torsional configuration we document the progressive evolution of talc microstructure up to shear strains of $\gamma = 8$ at pressures of 1 GPa and temperatures of 450–500°C, similar to a hot subduction zone environment such as Cascadia (Currie et al., 2004) (Figure 1). Specimens were deformed at constant shear strain rates comparable to deformation rates imposed during SSEs (Rowe et al., 2011).

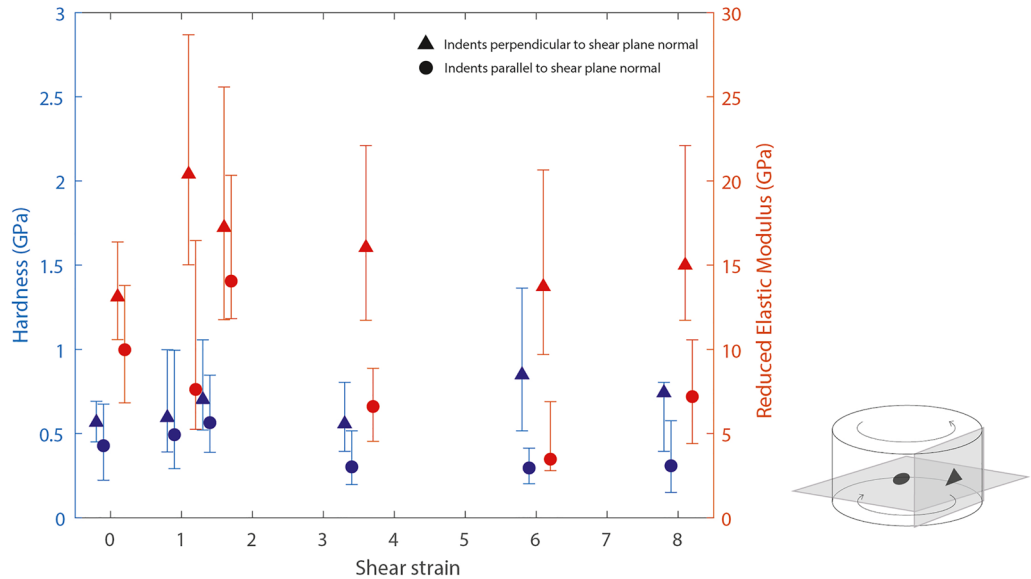


**Figure 4.** Nanoindentation results for indents made both with the loading axis parallel to the shear plane normal (circles) and with the loading axis perpendicular to the shear plane normal (triangles) (see inset on lower right-hand side). Indentation hardness is depicted in blue (left hand *y* axis) and reduced elastic modulus is depicted in red (right hand *y* axis). Each point on the graph corresponds to the median and 10:90% confidence intervals for approximately 200 data points. Clusters of data at each experimental strain are offset for clarity. The hardness does not evolve significantly within error, remaining low across all sample strains. Conversely, the reduced elastic modulus reveals a developing anisotropy as strain in the starting material increases, a phenomenon which we attribute to ripplocations and delaminations occurring preferentially within the shear plane.

Observations of delaminations and ripplocations in the TEM images require the separation and sliding of crystal lattices, resulting in the creation of void space, phenomena which are neither fully brittle nor fully plastic. Furthermore, we do not observe any definitive microstructural evidence for viscoplastic creep, such as grain boundary migration or the nucleation and growth of strain-free grains (Tullis, 2002). However, the formation of kinked grains (as described in Escartín et al. (2008)) is accommodated by plastic deformation. Therefore, we interpret the observed behavior as semi-brittle.

Previous experimental work has characterized deformation microstructures for talc at lower pressures, yet these studies still document many of the same microstructures we observe here. As in the experiments performed by Escartín et al. (2008) and Misra et al. (2014), we observe a portion of the strain that is accommodated by the development of kinked grains (Figure 3). Furthermore, the (001) delaminations described by Escartín et al. (2008) are also clearly visible in all deformed specimens, but increase in frequency with accumulated strain (Figure 3). In addition, many of these deformation features described herein have also been observed in naturally deformed specimens exhumed along low-angle detachment faults (Collettini et al., 2009; Viti & Collettini, 2009). For example, the core of the continental Zuccale fault on the Isle of Elba, Italy, which was active at <8 km depth (Musumeci et al., 2015), contains pockets of naturally deformed, interconnected talc domains (Collettini et al., 2009; Viti & Collettini, 2009). Microstructural observations of these natural samples reveal grain sizes and (001) delaminations similar to observations of our high-strain samples (Figure 3). Finally, we also observe the formation of ripplocations (Kushima et al., 2015), especially at higher strains (Figure 3). Ripplocations are a newly described phenomenon that help to explain how layered materials can accommodate strain without cracking, and have also been described recently in the mineral biotite, another layered silicate (Aslin et al., 2019). In concordance with prior studies at lower pressures (Collettini et al., 2009; Escartín et al., 2008; Misra et al., 2014; Viti & Collettini, 2009), we conclude that temperature-dependent plastic deformation accommodated solely by dislocation motion may not become relevant for talc up to pressures of at least 1 GPa. Rather, frictional slip along planar defects such as grain boundaries is likely to control the strength of talc-bearing rocks deep within subduction zones. This result is in agreement with an earlier high pressure study on talc (Edmond & Paterson, 1971), which did not document deformation microstructures but reported mechanical data suggestive of brittle or semi-brittle behavior up to at least 0.8 GPa. More recently, Boneh et al. (2023)

performed a low strain, high pressure study on talc which also detailed both microstructural and mechanical evidence for a semi-brittle talc rheology. Porosity generated by delaminations, kinking, and ripplocations could also provide pathways for fluids to continue permeating fault zones even after faults have been active for a long time at relatively high pressures. Since it is geometrically necessary for the talc to experience a shear stress in order to form porosity in the form of kink hinges and ripplocations, these features cannot simply be the artifacts of decompression of the experimental samples. Therefore, these void spaces were likely open to some degree even at high pressure. Recent work on exhumed subduction zone material has suggested that talc under conditions of high pore fluid pressure could become important for both slow slip and creep events at the subduction zone interface (French & Condit, 2019). The nanoporosity we observe could allow for the high pore fluid pressures required for these phenomena to take place. Conversely, an increase in porosity could lead to a drop in pore fluid pressure, potentially enabling a self-arresting mechanism for such seismic events as has been observed in real world slow earthquakes (e.g., Wei et al., 2021). In addition to facilitating fluid migration, these pore spaces could also provide accommodating spaces for pressure solution creep, another deformation mechanism that may be important in subduction zone settings (Condit & French, 2022; Fagereng & Den Hartog, 2017). It is possible that these voids could be filled by talc crystal growth or other precipitates from the fluid itself. However, under active deformation conditions we expect new void spaces to continue opening up as long as the talc continues to undergo shearing.

Berkovich nanoindentation, due to its pyramidal geometry, produces a complex strain-state that in most crystalline materials requires the simultaneous activity of multiple slip systems (Fischer-Cripps, 2004). Considering the deformation microstructures of the high temperature torsion experiments, we suggest that nanoindentation in talc also induces a semi-brittle response. Therefore, it is assumed that frictional slip along planar defects such as grain boundaries is the main control on the hardness of talc-bearing rocks, and that the indentation hardnesses presented herein reflect a semi-brittle, rather than a plastic, control on rock strength. We find that indents in talc yield low hardnesses and reduced elastic moduli across all strains (Figure 4), values which are comparable to prior studies (Broz et al., 2006). Notably, the hardness does not evolve significantly as strain and microstructural damage accumulate. This is likely due to talc's low coefficient of internal friction, which is approximately equal to the coefficient of sliding friction (Escartín et al., 2008).

We also observed the development of a large anisotropy in the reduced elastic modulus, with indents parallel to the shear plane normal consistently returning lower values (Figure 4). We attribute this anisotropy to delaminations and ripplocations opening void space parallel to the (001) planes, which are increasingly aligned within the shear plane as deformation progresses. Although the microstructural damage is significant, we see little evidence for the weakening of talc with progressive strain. Therefore, talc-rich shear zones are not expected to undergo protracted rheological changes during high strain deformation. This is in contrast to the transition from grain size insensitive to grain size sensitive deformation mechanisms that is observed in shear zones composed from different minerals, facilitating weakening (Warren & Hirth, 2006). The specific deformation behavior of talc could allow it to weaken faults at low pressures but may contribute to increased fault strength at higher pressures because of the apparent absence of fully plastic deformation mechanisms.

## 5. Conclusion

Since talc is an important mineralogical component of many faults, understanding its deformation behavior and rheology are important for understanding fault zone processes and associated geohazards. The microstructures observed in the experiments herein strongly suggest that talc does not undergo a brittle-to-plastic transition across a large proportion of the seismically active regions of a subduction zone. Instead, talc remains a semi-brittle material across a wide range of relevant subduction zone temperatures, pressures, and deformation rates. However, the porosity generated by delaminations and ripplocations could supply additional pathways for fluids to migrate through the fault zone. Increased porosity and permeability may also enhance deformation by pressure solution creep, although further experiments are needed to investigate this phenomenon. These conclusions provide experimental support for prior field studies of exhumed subduction faults (French & Condit, 2019), which suggested that talc-rich lithologies would become important for hosting SSEs only under conditions whereby the pore fluid pressures approach lithostatic pressure. Although the low frictional coefficient of talc has frequently been hypothesized to weaken fault cores (Collettini et al., 2009; Giorgetti et al., 2015; Hirauchi et al., 2013; Moore & Lockner, 2008; Moore & Rymer, 2007) at shallow depths, under the high pressures of a deep subduction

zone interface, deformation and associated seismicity within talc-bearing lithologies continues to be enabled by void-producing, semi-brittle phenomena.

## Conflict of Interest

The authors declare no conflicts of interest relevant to this study.

## Data Availability Statement

The nanoindentation metadata files for the data presented in this work are archived in the Open Scholarship repository service provided by the Washington University in St. Louis libraries (DOI: https://doi.org/10.7936/fn25-bp23), and can be accessed at the following URL: https://openscholarship.wustl.edu/data/103/

**Acknowledgments**
This research was supported by NSF grant EAR-1848824 awarded to Philip Skemer. Instrumentation support was provided by the Institute of Materials Science and Engineering at Washington University in St Louis. Special thanks go to Guodong Ren, Rohan Mishra, Mike Sly, and Kate Padilla for lending their technical expertise, and Katharine Flores for use of the nanoindentation facility. In addition, we would like to thank Haemyeong Jung for advice regarding sample preparation, and Doug Wiens for engaging in many useful discussions. Finally, we thank Telemaco Tesei and Cailey Condit for their thoughtful and thorough reviews that greatly improved the manuscript.

## References

Aslin, J., Mariani, E., Dawson, K., & Barsoum, M. W. (2019). Ripplocations provide a new mechanism for the deformation of phyllosilicates in the lithosphere. *Nature Communications*, *10*(1), 1–9. https://doi.org/10.1038/s41467-019-08587-2

Bonatti, E., Honnorez, J., & Ferrara, G. (1971). Peridotite-gabbro-basalt complex from the equatorial mid-Atlantic ridge. *Philosophical Transactions of the Royal Society A: Mathematical, Physical & Engineering Sciences*, *268*(1192), 385–402.

Boneh, Y., Pec, M., & Hirth, G. (2023). High-pressure mechanical properties of talc—Implications for fault strength and slip processes. *Journal of Geophysical Research: Solid Earth*, *128*(3), e2022JB025815. https://doi.org/10.1029/2022JB025815

Boschi, C., Früh-Green, G. L., & Escartín, J. (2006). Occurrence and significance of serpentinite-hosted, talc- and amphibole-rich fault rocks in modern oceanic settings and ophiolite complexes: An overview. *Ofioliti*, *31*(2), 129–140.

Brace, W. F., Walsh, J. B., & Frangos, W. T. (1968). Permeability of granite under high pressure. *Journal of Geophysical Research*, *73*(6), 2225–2236. https://doi.org/10.1029/jb073i006p02225

Broz, M. E., Cook, R. F., & Whitney, D. L. (2006). Microhardness, toughness, and modulus of Mohs scale minerals. *American Mineralogist*, *91*(June), 135–142. https://doi.org/10.2138/am.2006.1844

Bürgmann, R. (2018). The geophysics, geology and mechanics of slow fault slip. *Earth and Planetary Science Letters*, *495*, 112–134. https://doi.org/10.1016/j.epsl.2018.04.062

Byerlee, J. D. (1978). Friction of rocks (p. 116).

Collettini, C., Viti, C., Smith, S. A., & Holdsworth, R. E. (2009). Development of interconnected talc networks and weakening of continental low-angle normal faults. *Geology*, *37*(6), 567–570. https://doi.org/10.1130/G25645A.1

Condit, C. B., & French, M. E. (2022). Geologic evidence of lithostatic pore fluid pressures the base of the subduction seismogenic zone. *Geophysical Research Letters*, *49*(12), e2022GL098862. https://doi.org/10.1029/2022gl098862

Cross, A. J., & Skemer, P. (2017). Ultramylonite generation via phase mixing in high-strain experiments. *Journal of Geophysical Research: Solid Earth*, *122*(3), 1744–1759. https://doi.org/10.1002/2016JB013801

Currie, C. A., Wang, K., Hyndman, R. D., & He, J. (2004). The thermal effects of steady-state slab-driven mantle flow above a subducting plate: The Cascadia subduction zone and backarc. *Earth and Planetary Science Letters*, *223*(1–2), 35–48. https://doi.org/10.1016/j.epsl.2004.04.020

Edmond, J. M., & Paterson, M. S. (1971). Strength of solid pressure media and implications for high pressure apparatus. *Contributions to Mineralogy and Petrology*, *30*(2), 141–160. https://doi.org/10.1007/BF00372255

Escartín, J., Andreani, M., Hirth, G., & Evans, B. (2008). Relationships between the microstructural evolution and the rheology of talc at elevated pressures and temperatures. *Earth and Planetary Science Letters*, *268*(3–4), 463–475. https://doi.org/10.1016/j.epsl.2008.02.004

Escartín, J., Mével, C., MacLeod, C. J., & McCaig, A. M. (2003). Constraints on deformation conditions and the origin of oceanic detachments: The mid-Atlantic ridge core complex at 15°45′N. *Geochemistry, Geophysics, Geosystems*, *4*(8), 1067. https://doi.org/10.1029/2002GC000472

Fagereng, Å., & Den Hartog, S. A. M. (2017). Subduction megathrust creep governed by pressure solution and frictional-viscous flow. *Nature Geoscience*, *10*(1), 51–57. https://doi.org/10.1038/ngeo2857

Fischer-Cripps, A. (2004). *Nanoindentation, mechanical engineering series*. Springer Science+Business Media, LLC. https://doi.org/10.1115/1.1704625

French, M. E., & Condit, C. B. (2019). Slip partitioning along an idealized subduction plate boundary at deep slow slip conditions. *Earth and Planetary Science Letters*, *528*, 115828. https://doi.org/10.1016/j.epsl.2019.115828

Giorgetti, C., Carpenter, B. M., & Collettini, C. (2015). Frictional behavior of talc-calcite mixtures. *Journal of Geophysical Research: Solid Earth*, *120*(9), 6614–6633. https://doi.org/10.1002/2015JB011970.Received

Hirauchi, K. I., den Hartog, S. A. M., & Spiers, C. J. (2013). Weakening of the slab-mantle wedge interface induced by metasomatic growth of talc. *Geology*, *41*(1), 75–78. https://doi.org/10.1130/G33552.1

Hyndman, R. D., Yamano, M., & Oleskevich, D. (1997). The seismogenic zone of subduction thrust faults. *Island Arc*, *6*(3), 244–260. https://doi.org/10.1111/j.1440-1738.1997.tb00175.x

Kim, Y., Clayton, R. W., Asimow, P. D., & Jackson, J. M. (2013). Generation of talc in the mantle wedge and its role in subduction dynamics in central Mexico. *Earth and Planetary Science Letters*, *384*, 81–87. https://doi.org/10.1016/j.epsl.2013.10.006

King, R. L., Kohn, M. J., & Eiler, J. M. (2003). Constraints on the petrologic structure of the subduction zone slab-mantle interface from Franciscan Complex exotic ultramafic blocks. *GSA Bulletin*, *115*(9), 1097–1109. https://doi.org/10.1130/b25255.1

Kushima, A., Qian, X., Zhao, P., Zhang, S., & Li, J. (2015). Ripplocations in van der Waals layers. *Nano Letters*, *15*(2), 1302–1308. https://doi.org/10.1021/nl5045082

Misra, S., Boutareaud, S., & Burg, J. P. (2014). Rheology of talc sheared at high pressure and temperature: A case study for hot subduction zones. *Tectonophysics*, *610*, 51–62. https://doi.org/10.1016/j.tecto.2013.10.009

Moore, D., & Lockner, D. A. (2011). Frictional strengths of talc—Serpentine and talc—Quartz mixtures. *Journal of Geophysical Research*, *116*(B1), 1–17. https://doi.org/10.1029/2010JB007881

Moore, D. E., & Lockner, D. (2008). Talc friction in the temperature range 25–400C: Relevance for fault-zone weakening. *Tectonophysics*, *449*(1–4), 120–132. https://doi.org/10.1016/j.tecto.2007.11.039

Moore, D. E., & Rymer, M. (2007). Talc-bearing serpentinite and the creeping section of the San Andreas fault. *Nature*, *448*(7155), 795–797. https://doi.org/10.1038/nature06064

Morrow, C., Moore, D., & Lockner, D. (2000). The effect of mineral bond strength and adsorbed water on fault gouge frictional strength. *Geophysical Research Letters*, *27*(6), 815–818. https://doi.org/10.1029/1999GL008401

Musumeci, G., Mazzarini, F., & Cruden, A. R. (2015). The Zuccale fault, Elba Island, Italy: A new perspective from fault architecture. *Tectonics*, *34*(6), 1195–1218. https://doi.org/10.1002/2014TC003809

Paterson, M. S. (1958). Experimental deformation and faulting in wombeyan marble. *Bulletin of the Geological Society of America*, *69*(April), 465–476. https://doi.org/10.1130/0016-7606(1958)69[465:edafiw]2.0.co;2

Pawley, A. R., & Wood, B. J. (1995). The high-pressure stability of talc and 10 Å phase: Potential storage sites for $H_2O$ in subduction zones. *American Mineralogist*, *80*(9–10), 998–1003. https://doi.org/10.2138/am-1995-9-1015

Rowe, C. D., Meneghini, F., & Casey Moore, J. (2011). Textural record of the seismic cycle: Strain-rate variation in an ancient subduction thrust. *Geological Society - Special Publications*, *359*(1), 77–95. https://doi.org/10.1144/SP359.5

Schwartz, S. Y., & Rokosky, J. M. (2007). Slow slip events and seismic tremor at circum-Pacific subduction zones. *Review of Geophysics*, *45*(3), 1–32. https://doi.org/10.1029/2006RG000208.1

Sly, M. K., Thind, A. S., Mishra, R., Flores, K. M., & Skemer, P. (2020). Low-temperature rheology of calcite. *Geophysical Journal International*, *221*(1), 129–141. https://doi.org/10.1093/gji/ggz577

Spandler, C., Hermann, J., Faure, K., Mavrogenes, J. A., & Arculus, R. J. (2008). The importance of talc and chlorite "hybrid" rocks for volatile recycling through subduction zones; evidence from the high-pressure subduction mélange of New Caledonia. *Contributions to Mineralogy and Petrology*, *155*(2), 181–198. https://doi.org/10.1007/s00410-007-0236-2

Syracuse, E. M., van Keken, P. E., & Abers, G. A. (2010). The global range of subduction zone thermal models. *Physics of the Earth and Planetary Interiors*, *183*(1–2), 73–90. https://doi.org/10.1016/j.pepi.2010.02.004

Tullis, J. (2002). Deformation of granitic rocks: Experimental studies and natural examples. *Reviews in Mineralogy and Geochemistry*, *51*(1), 51–95. https://doi.org/10.2138/gsrmg.51.1.51

Viti, C., & Collettini, C. (2009). Growth and deformation mechanisms of talc along a natural fault: A micro/nanostructural investigation. *Contributions to Mineralogy and Petrology*, *158*(4), 529–542. https://doi.org/10.1007/s00410-009-0395-4

Warren, J. M., & Hirth, G. (2006). Grain size sensitive deformation mechanisms in naturally deformed peridotites. *Earth and Planetary Science Letters*, *248*(1–2), 438–450. https://doi.org/10.1016/j.epsl.2006.06.006

Wei, X., Xu, J., Liu, Y., & Chen, X. (2021). The slow self-arresting nature of low-frequency earthquakes. *Nature Communications*, *12*(1), 1–9. https://doi.org/10.1038/s41467-021-25823-w

Wibberley, C. (2007). Seismology: Talc at fault. *Nature*, *448*(7155), 756–757. https://doi.org/10.1038/448756a